International Symposium
On Turbulence and Shear Flow
Phenomena (TSFP-9)
June 30 - July 3, 2015 *Melbourne, Australia*

CHARACTERISTICS OF PRESSURE DISTRIBUTION AND SKIN FRICTION WITHIN THE LAMINAR SEPARATION BUBBLE AT DIFFERENT REYNOLDS NUMBERS

Donghwi Lee
Dept. of Aeronautics and Astronautics, University of Tokyo
3-1-1 Yoshinodai, Sagamihara, Kanagawa 252-5210, Japan
lee@flab.isas.jaxa.jp

Soshi Kawai, Taku Nonomura, Akira Oyama, and Kozo Fujii
Dept. of Space Flight System
Institute of Space and Astronautical Science, Japan Aerospace Exploration Agency
3-1-1 Yoshinodai, Sagamihara, Kanagawa 252-5210, Japan

ABSTRACT

Mechanisms behind the pressure distribution within a laminar separation bubble (LSB) are investigated by large-eddy simulations around a 5% thickness blunt flat plate. The plate length based Reynolds numbers are set to be (Re_c) 5.0×10^3, 6.1×10^3, 8.0×10^4, 1.1×10^4, and 2.0×10^4. From the results, two types of LSB are observed; steady laminar separation bubble (LSB_S) at $Re_c = 5.0\times10^3$ and 6.1×10^3, and a steady-fluctuating laminar separation bubble (LSB_SF) at $Re_c = 8.0\times10^3$, 1.1×10^4, and 2.0×10^4. As the Reynolds number increases, different shapes of pressure disribution appear such that a gradual pressure recovery in the LSB_S and a plateau pressure distribution followed by a rapid pressure recovery in the LSB_SF. The reasons of appearing the different shapes of pressure distributions depending on the Reynolds number are explained by deriving the Reynolds averaged pressure gradient equation. From the momentum budgets of the equation, it is confirmed that the viscous stress near the surface has an influence on determining the different shape of pressure distribution. The different viscous stress distributions near the surface are affected by grwoth of the separated laminar shear layer depending on the Reynolds number or generation of the Reynolds shear stress.

INTRODUCTION

A laminar separation bubble (LSB) shown in Fig. 1 is formed through the laminar boundary layer separation, transition and reattachement process. The LSB appears in many practical flows such as turbine blades or micro air vehicle airfoils. When the LSB is formed, it is often observed that a plateau pressure distribution appears from the separation to transition point and a rapid pressure recovery occurs from the transition to reattachment point. This plateau pressure distribution has been often considered as a general characteristic of the LSB (Tani (1964); Horton (1968); Carmichael (1982); Lissaman (1983)).

In respect of the pressure distribution around the LSB, Anyoji *et al.* (2011) have reported interesting experimental resutls. They measured surface pressure distribution of a 5% thickness blunt flat plate at zero incidence at the plate length based Reynolds numbers of $Re_c = 4.9\times10^3$, 6.1×10^3, 1.1×10^4, 2.0×10^4 and 4.1×10^4. From the results, the LSBs have been formed in all cases but different pressure distributions have been observed depending on the Reynolds numbers. At the lower Reynolds numbers ($Re_c = 4.9\times10^3$ and 6.1×10^3), a gradual pressure recovery without showing the plateau pressure distribution has been observed which does not commonly appear in pressure distributions around the LSB. At relatively higher Reynolds number ($Re_c \geq 1.1\times10^4$), the pressure distributions begin to show the general shapes such as the plateau region with the rapid pressure recovery. These results have suggested that the plateau pressure distribution is not a common feature of the LSB and some characteristics of the flows make the differences of the pressure distribution. However, the physical understandings of appearing these different pressure distributions within the LSB are not sufficient. Therefore, in this study, large-eddy simulations are performed to understand characteristics of the LSB and to reveal the physical mechanisms of the surface pressure skin friction distributions within the LSB region.

COMPUTATIONAL SETUP

Computational Method

The spatial derivatives of the convective and viscous terms are evaluated by the 6^{th}-order compact difference scheme (Lele (1992)) with the 10^{th}-order low-pass filtering (Lele (1992); Gaitonde & Visbal (2000)). The 2nd-order backward differencing converged by alternate directional implicit symmetric Gauss Seidel (ADI-SGS) (Fujii (1998)) and five subiterations (Chakravarthy (1984)) are adopted for time integration. The computational time step Δt is $2.0\times10^{-4}s$. Although many methods representing subgrid-scale (SGS) effects are proposed, Kawai *et al.* (2010) have reported that the high order numerics with sufficient grid

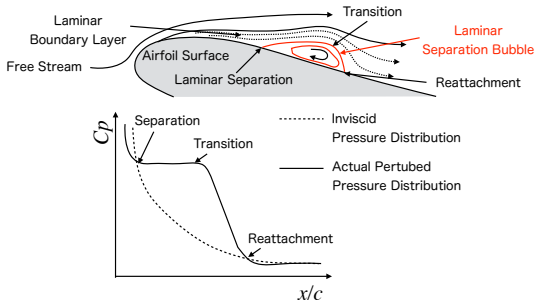

Figure 1. Laminar separation bubble and surface pressure distribution (redrawn by referring Roberts (1980)).

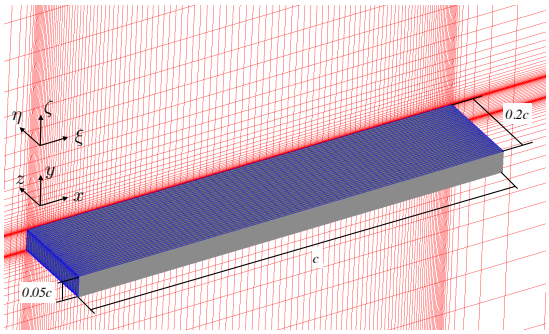

Figure 2. Computational grid for a 5% thickness flat plate.

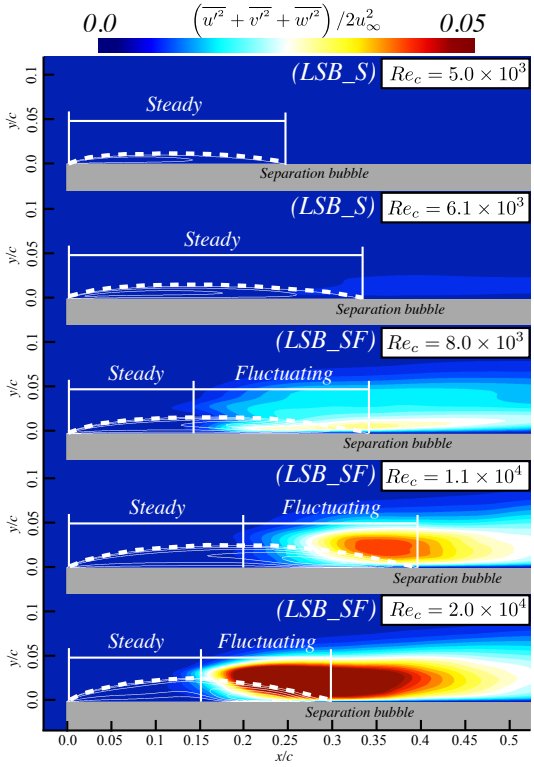

Figure 3. Turbulent Kinetic Energy flow fields.

resolution without SGS model showed better resolution for turbulence. Therefore, an implicit approach in which no explicit SGS model is used in this study.

Computational Grid and Conditions

Figure 2 shows a single zone orthogonal grid around a 5% thickness blunt leading edge flat plate. The physical properties inside the flat plate are not used when the spatial difference is calculated. The outer boundary is extended to 25 times of the chord length and the spanwise domain size is employed 20% of the chord length with the periodic boundary condition. Non-slip, and adiabatic conditions are adopted on the surface. The free-stream Mach number M_∞ with zero free-stream turbulence level, specific heat ratio γ, and Prandtl number Pr are set to be 0.2, 1.4, and 0.72, respectively. The Re_c are set to be 5.0×10^3, 6.1×10^3, 8.0×10^3, 1.1×10^4, and 2.0×10^4. The number of total grid points in streamwise, wall-normal, and spanwise directions are $N_x\times N_y\times N_z = 471\times359\times101$.

RESULT AND DISCUSSION

The statistical data obtained by time- and spanwise-averaging in a quasi-steady state will be used from the following discussion. The time- and spanwise-averaged, and fluctuating contributions are denoted by $\overline{f}$ and f' for any instantaneous flow variable f, respectively (i.e., $f=\overline{f}+f'$).

Characteristics of the Separation Bubbles

Figure 3 shows turbulent kinetic energy (T.K.E.) fields. The flow fields considered in this study separate from a leading edge and reattach in the middle of the flat plate, consequently the LSB is formed in all Re_c cases. The formation of LSB is also shown in Fig. 3 The T.K.E. is negligibly small (smaller than $0.002u_\infty$) at the lower Reynolds numbers ($Re_c = 5.0\times10^3$ and 6.1×10^3) within the entire LSB region. This type of LSB is called as a steady laminar separation bubble (LSB_S) in this study. At the higher Reynolds numbers ($Re_c = 8.0\times10^3$, 1.1×10^4 and 2.0×10^4), on the other hand, the characteristics of the LSB show two region. The first region is that the T.K.E. is approximately zero ($0.0\le x/c\le0.15$ at $Re_c = 8.0\times10^3$, $0.0\le x/c\le0.20$ at $Re_c = 1.1\times10^4$, and $0.0\le x/c\le0.15$ at $Re_c = 2.0\times10^4$), as similar to the LSB_S. Fluctuating region appears after the steady region ($0.15\le x/c\le0.35$ at $Re_c = 8.0\times10^3$, $0.20\le x/c\le0.40$ at $Re_c = 1.1\times10^4$, and $0.15\le x/c\le0.30$ at $Re_c = 2.0\times10^4$). In other words, the steady and fluctuating parts coexist within the LSB, so this type of LSB as a steady-fluctuating laminar separation bubble (LSB_SF) in this study.

Pressure Distribution & Skin Friction

Figure 4 shows the averaged surface pressure distribution ($\overline{C}_p$) and skin friction coefficient ($\overline{C}_f$) near the LSB. At the lower Reynolds numbers ($Re_c = 5.0\times10^3$ and 6.1×10^3, LSB_S), the gradual $\overline{C}_p$ without showing the plateau region appears and $\overline{C}_f$ also gradually increases toward the reattachment point. On the other hand, at the higher Reynolds numbers ($Re_c = 8.0\times10^3$, 1.1×10^4 and 2.0×10^4, LSB_SF), $\overline{C}_p$ begins to show the thypical plateau region which is often observed in many LSB studies (Lin & Pauley (1996); Anyoji *et al.* (2014)). In these cases, the plateau $\overline{C}_p$ is observed in the steady region ($0.0\le x/c\le0.15$ at $Re_c = 8.0\times10^3$, $0.0\le x/c\le0.20$ at $Re_c = 1.1\times10^4$, and $0.0\le x/c\le0.15$ at $Re_c = 2.0\times10^4$). The

rapid pressure recovery appears in the fluctuating region ($0.15 \le x/c \le 0.35$ at $Re_c = 8.0\times10^3$, $0.20 \le x/c \le 0.40$ at $Re_c = 1.1\times10^4$, and $0.15 \le x/c \le 0.30$ at $Re_c = 2.0\times10^4$). A negative peak on $\overline{C}_f$ appears near the fluctuating region. Interestingly, the $\overline{C}_p$ are different in the same steady flow region in the lower and higher Reynolds number cases. This fact indicates that the different $\overline{C}_p$ depending on the Reynolds numbers is affected by other factors rather than the steady flow condition.

Streamwise Pressure Gradient Equation

To reveal the physical mechanisms of the different $\overline{C}_p$ depending on the Reynolds numbers, an Reynolds averaged pressure gradient equation is derived from the streamwise momentum equation written as below.

$$\frac{\partial}{\partial t}(\rho u) + \frac{\partial}{\partial x_j}(\rho u u_j) = -\frac{\partial p}{\partial x} + \frac{1}{Re_c}\frac{\partial}{\partial x_j}\tau_{1j}\ ,\ (j=1,2,3), \tag{1}$$

where ρ and p are the density and static pressure, respectively. $u_j(\equiv u,v,w)$ are the velocity in each direction $x_j(\equiv x,y,z)$ and τ_{1j} is the viscous stress tensor for $j=1,2,3$. By considering averaged properties, the Reynolds averaged streamwise pressure gradient equation (Lee *et al.* (2015)) is

$$\frac{\partial \overline{p}}{\partial x} = -\frac{\partial}{\partial x_j}(\overline{\rho}\,\overline{u}\,\overline{u}_j) + \frac{1}{Re_c}\frac{\partial}{\partial x_j}\left(\mu\frac{\partial \overline{u}}{\partial x_j}\right) + \frac{1}{3}\frac{1}{Re_c}\frac{\partial}{\partial x}\left(\mu\frac{\partial \overline{u}_j}{\partial x_j}\right) + \frac{\partial}{\partial x_j}(-\overline{\rho}\overline{u'u'_j}) - \frac{\partial}{\partial x_j}T_{fluc}\ ,\ (j=1,2), \tag{2}$$

$$T_{fluc} = \overline{u}\overline{\rho'u'_j} + \overline{u}_j\overline{\rho'u'} + \overline{\rho'u'u'_j}\ ,\ (j=1,2). \tag{3}$$

We confirmed that Eq. (3) is negligible because the density fluctuation ρ' can be neglected. Therefore, the averaged streamwise pressure gradient term $\left(\frac{\partial \overline{p}}{\partial x}\right)$ equals to sum of the convective $\left(-\frac{\partial}{\partial x_j}(\overline{\rho}\,\overline{u}\,\overline{u}_j)\right)$, the first and second viscous diffusion $\left(\frac{1}{Re_c}\frac{\partial}{\partial x_j}\left(\mu\frac{\partial \overline{u}}{\partial x_j}\right), \frac{1}{3}\frac{1}{Re_c}\frac{\partial}{\partial x}\left(\mu\frac{\partial \overline{u}_j}{\partial x_j}\right)\right)$, and Reynolds shear stress terms $\left(\frac{\partial}{\partial x_j}(-\overline{\rho}\overline{u'u'_j})\right)$. The flow fields near the LSB of each term in the R.H.S. of Eq. (2) at each Reynolds number are shown in Fig. 5. From the discussion below, the results at $Re_c = 8.0\times10^3$ are omitted because the characteristics are similar to other LSB_SF cases. Within the steady LSB region near the surface, differences between the LSB_S and LSB_SF are clearly observed in the first viscous diffusion term as shown in Fig. 5(b). In the steady region of LSB_S, the first viscous diffusion effects exists near the surface and it is the dominant term for creating the gradual pressure recovery (i.e., $d\overline{p}/dx > 0$). On the other hand, in the steady region of LSB_SF, the first viscous diffusion but also the other terms can be ignored near the surface as the Reynolds number increases, and thus the plateau pressure distribution is created (i.e., $d\overline{p}/dx \simeq 0$). In the fluctuating region of LSB_SF, the convective and Reynolds shear stress effects are generated away from the surface, shown in Fig. 5(a), and (d). As a result, the strong viscous diffusion effects are created near the surface and makes the rapid pressure recovery (i.e., $d\overline{p}/dx \gg 0$).

The first viscous diffusion term which dominantly affects the streamwise pressure gradient can be decomposed into two terms,

$$\frac{1}{Re_c}\frac{\partial}{\partial x_j}\left(\mu\frac{\partial \overline{u}}{\partial x_j}\right) = \frac{1}{Re_c}\frac{\partial}{\partial x}\left(\mu\frac{\partial \overline{u}}{\partial x}\right) + \frac{1}{Re_c}\frac{\partial}{\partial y}\left(\mu\frac{\partial \overline{u}}{\partial y}\right). \tag{4}$$

We confirmed that the viscous diffusion mainly consists of the second term in the R.H.S. of Eq. (4), which stands for the normal stress in the wall-normal direction. Accordingly, the differences in the viscous diffusion effects at the different Reynolds number can be explained by the viscous stress $\left(\frac{\mu}{Re}\frac{\partial \overline{u}}{\partial y}\right)$ and velocity $(\overline{u})$ distributions. Therefore, from the following discussion, the quantitative analysis is shown by the contributions of each term in Eq. (2), and the velocity, viscous stress, and viscous diffusion profiles in the steady and fluctuating region.

Steady Region In the steady region of LSB_S and LSB_SF, different viscous stress near the surface is affected by the different growth of the separated laminar shear layer depending on the Reynolds number. Left side of Fig. 6 shows momentum budgets, and right side of Fig. 6 shows the velocity, viscous stress, and viscous diffusion profiles at several locations in the steady region of the LSB_S and LSB_SF. In the steady region of the LSB_S ($0.0 \le x/c \le 0.25$ at $Re_c = 5.0\times10^3$, and $0.0 \le x/c \le 0.33$ at 6.1×10^3), i.e., entire the LSB region, the progressively developed shear layer is formed by the low Reynolds number effects. It leads to the continous viscous stress near the surface and approximately constant viscous diffusion. Because the three terms of R.H.S. in Eq. (2) are negligibly small in the steady region near the surface, as already discussed in Fig. 5, the constant viscous diffusion distribution makes the R.H.S. of Eq. (2) positive. As a result, the favorable pressure gradient ($\partial\overline{p}/\partial x > 0$) without showing the plateau pressure distribution is generated within the LSB. Additionally, because of reducing the effects of the viscous stress as going to the downstream, $\overline{C}_f$ gradually increases toward the reattachment point.

In the steady region of the LSB_SF ($0.0 \le x/c \le 0.20$ at $Re_c = 1.1\times10^4$, and $0.0 \le x/c \le 0.15$ at $Re_c = 2.0\times10^4$), on the other hand, relatively thin shear layers are generated by the higher Reynolds number effect, and the viscous stress near the surface becomes considerably smaller than the LSB_S cases. As a result, effect of the viscous diffusion near the surface becomes negligibly small. In other words, all terms of R.H.S. in Eq. (2) are approximately zero and the plateau pressure distributions are created ($\partial\overline{p}/\partial x \simeq 0$). Therefore, the different shapes of the pressure distribution in the steady region of the LSB_S and LSB_SF are caused by the different viscous stress distribution. The different viscous stress distributions depending on the Reynolds number come from differences of the separated laminar shear layer development.

Fluctuating Region The flow states of the LSB_S are steady within the entire LSB and the fluctuating region only appears in the LSB_SF. Left side of Fig. 7 shows momentum budgets, and right side of Fig. 7 shows the velocity, viscous stress, and viscous diffusion profiles at several locations in the fluctuating region of the LSB_SF. In the fluctuating region of the LSB_SF ($0.20 \le x/c \le 0.40$ at $Re_c = 1.1\times10^4$, and $0.15 \le x/c \le 0.30$ at $Re_c = 2.0\times10^4$), the convective and Reynolds stress terms contribute to the

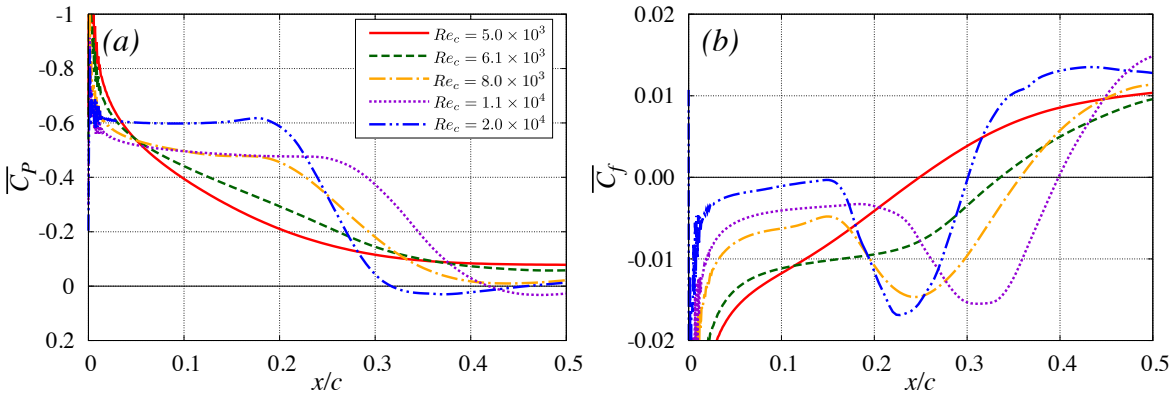

Figure 4. The time- and spanwise-averaged (a) surface pressure distribution and (b) skin friction coefficient.

high pressure gradient away from the surface. When we only focus on near the surface, however, the strong viscous stress is generated near the surface, and it creates the negative peak value on $\overline{C}_f$. Moreover, the strong viscous diffusion makes the R.H.S. of Eq. (2) larger than zero. Thus, a high pressure gradient is created ($\partial\overline{p}/\partial x \gg 0$), which stands for the rapid pressure recovery. It can be considered that the strong viscous stress which leads to high viscous diffusion near the surface is generated to balance with the Reynolds stress away from the surface. Thereby, the presence of fluctuating components plays an important role in the rapid pressure recovery process.

CONCLUSION

Large-eddy simulations around the 5% thickness blunt flat plate at plate lentgh based Reynolds number $Re_c = 5.0 \times 10^3$, 6.1×10^3, 8.0×10^3, 1.1×10^4 and 2.0×10^4 were performed to understand the physical mechanisms of the surface pressure distribution ($\overline{C}_p$) and skin friction coefficient ($\overline{C}_f$) within the laminar separation bubble (LSB). First of all, two types of LSBs are classified depending on the Reynolds number such as the steady laminar separation bubble (LSB_S) at lower Reynolds numbers ($Re_c = 5.0 \times 10^3$ and 6.1×10^3), and steady-fluctuating laminar separation bubble (LSB_SF) at relatively higher Reynolds numbers ($Re_c = 8.0 \times 10^3$, 1.1×10^4, and 2.0×10^4). In the LSB_S, the gradual $\overline{C}_p$ recovery without showing the plateau region is observed. On the other hand, the plateau region before the rapid $\overline{C}_p$ recovery appears in the LSB_SF. From the momentum budget of the Reynolds averaged streamwise pressure gradient equation, it is confirmed that the viscous diffusion near the surface has a dominant influence to the different $\overline{C}_p$ between the LSB_S and LSB_SF. In the LSB_S, the progressively developed shear layer is formed due to the lower Reynolds number effects and the viscous stress cannot be neglected near the surface. Thus, the continuous viscous diffusion and gradual $\overline{C}_p$ recovery ($\partial\overline{p}/\partial x > 0$) are generated. In the steady region of LSB_SF, relatively thin shear layer is generated and the viscous stress can be ingored near the surface. Accordingly, it makes $\overline{C}_p$ become approximately zero, which means the constant pressure distribution ($\partial\overline{p}/\partial x \simeq 0$) is craeted. Moreover, in the fluctuating region of LSB_SF, the presence of fluctuating components due to the Reynolds stress induce the strong viscous stress near the surface and the rapid pressure recovery ($\partial\overline{p}/\partial x \gg 0$) is generated.

REFERENCES

Anyoji, M., Nonomura, T., Aono, H., Oyama, A., Fujii, K., Nagai, H. & Asai, K. 2014 Computational and experimental analysis of a high-performance airfoil under low-Reynolds-number flow condition. *J. Aircr.* **51** (6), 1864–1872.

Anyoji, M., Nose, K., Ida, S., Numata, D., Nagai, H. & Asai, K. 2011 Aerodynamic measurements in the Mars wind tunnel at Tohoku university. In *49th AIAA Aerosp. Sci. Meet. Incl. New Horizons Forum Aerosp. Expo.*. Orlando, FL: AIAA 2011-0852.

Carmichael, B. H. 1982 Low Reynolds number airfoil survey. *Tech. Rep.*. NASA-CR-165803.

Chakravarthy, S. R. 1984 Relaxation methods for unfactored implicit upwind schemes. In *22nd AIAA Aerosp. Sci. Meet.*. Reno, Nevada: AIAA 84-0165.

Fujii, K. 1998 Simple ideas for the accuracy and efficiency improvement of the compressible flow simulation methods. In *Proc. Int. CFD Work. Supersonic Transp. Des.*, pp. 20–23. Tokyo, Japan.

Gaitonde, D. V. & Visbal, M. R. 2000 Pade-type higher-order boundary filters for the Navier-Stokes equations. *AIAA J.* **38** (11), 2103–2112.

Horton, H. P. 1968 Laminar separation bubbles in two- and three-dimensional incompressible flow. Ph. d. thesis, University of London.

Kawai, S., Shankar, S. K. & Lele, S. K. 2010 Assessment of localized artificial diffusivity scheme for large-eddy simulation of compressible turbulent flows. *J. Comput. Phys.* **229** (5), 1739–1762.

Lee, D., Kawai, S., Nonomura, T., Anyoji, M., Aono, H., Oyama, A., Asai, K. & Fujii, K. 2015 Mechanisms of surface pressure distribution within a laminar separation bubble at different Reynolds numbers. *Phys. Fluids* **27** (023602).

Lele, S. K. 1992 Compact finite difference schemes with spectral-like resolution. *J. Comput. Phys.* **103** (1), 16–42.

Lin, J. C. M. & Pauley, Laura L. 1996 Low-Reynolds-number separation on an airfoil. *AIAA J.* **34** (8), 1570–1577.

Lissaman, P. B. S. 1983 Low-Reynolds-number airfoils. *Annu. Rev. Fluid Mech.* pp. 223–240.

Roberts, W. B. 1980 Calculation of laminar separation bubbles and their effect on airfoil performance. *AIAA J.* **18** (1), 25–31.

Tani, I. 1964 Low speed flows involving bubble separations. *Prog. Aerosp. Sci.* **5**, 70–103.

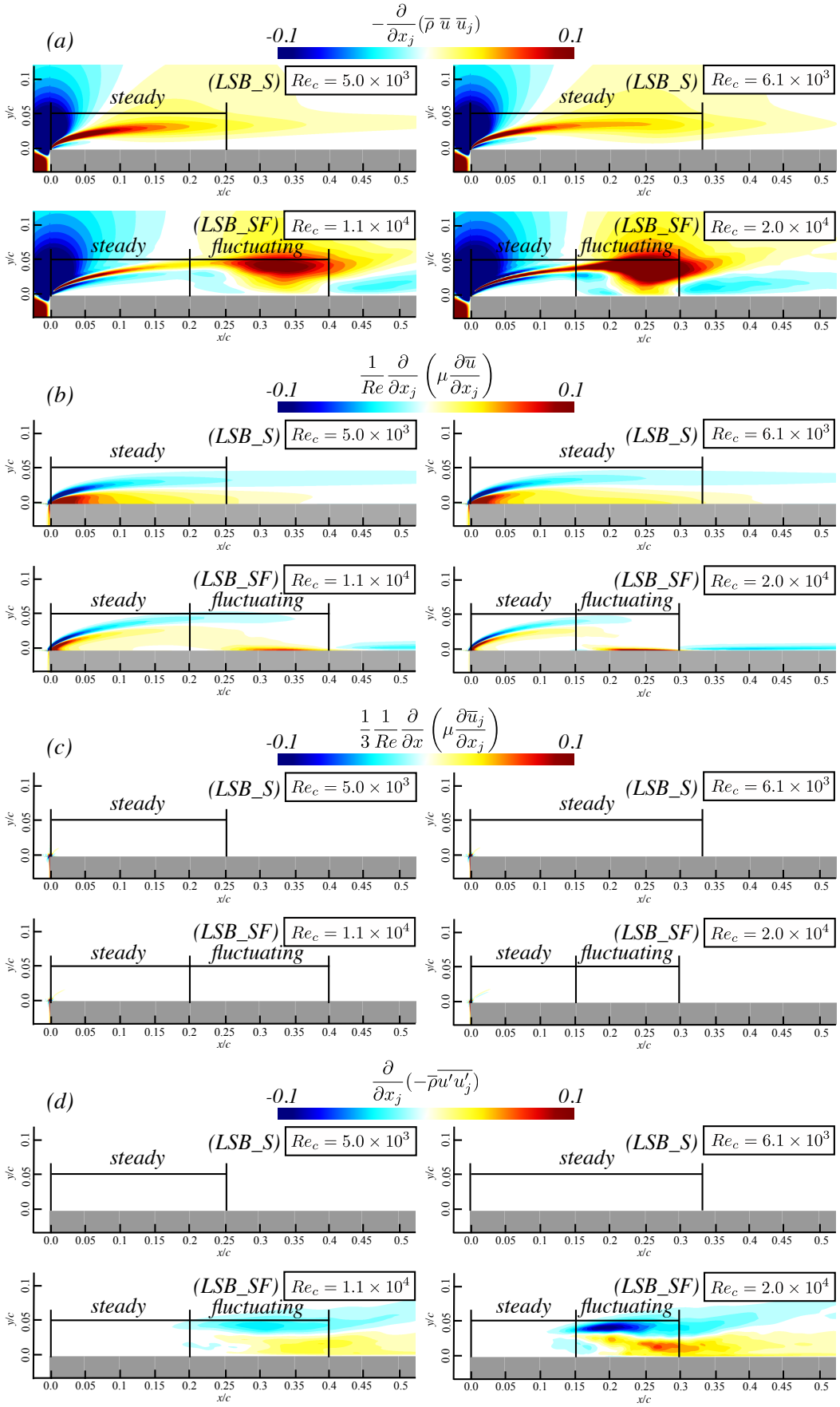

Figure 5. Flow fields of each term in the R.H.S. of Eq. (2). (a) convective, (b) first viscous diffusion, (c) second viscous diffusion, and (d) Reynolds stress terms.

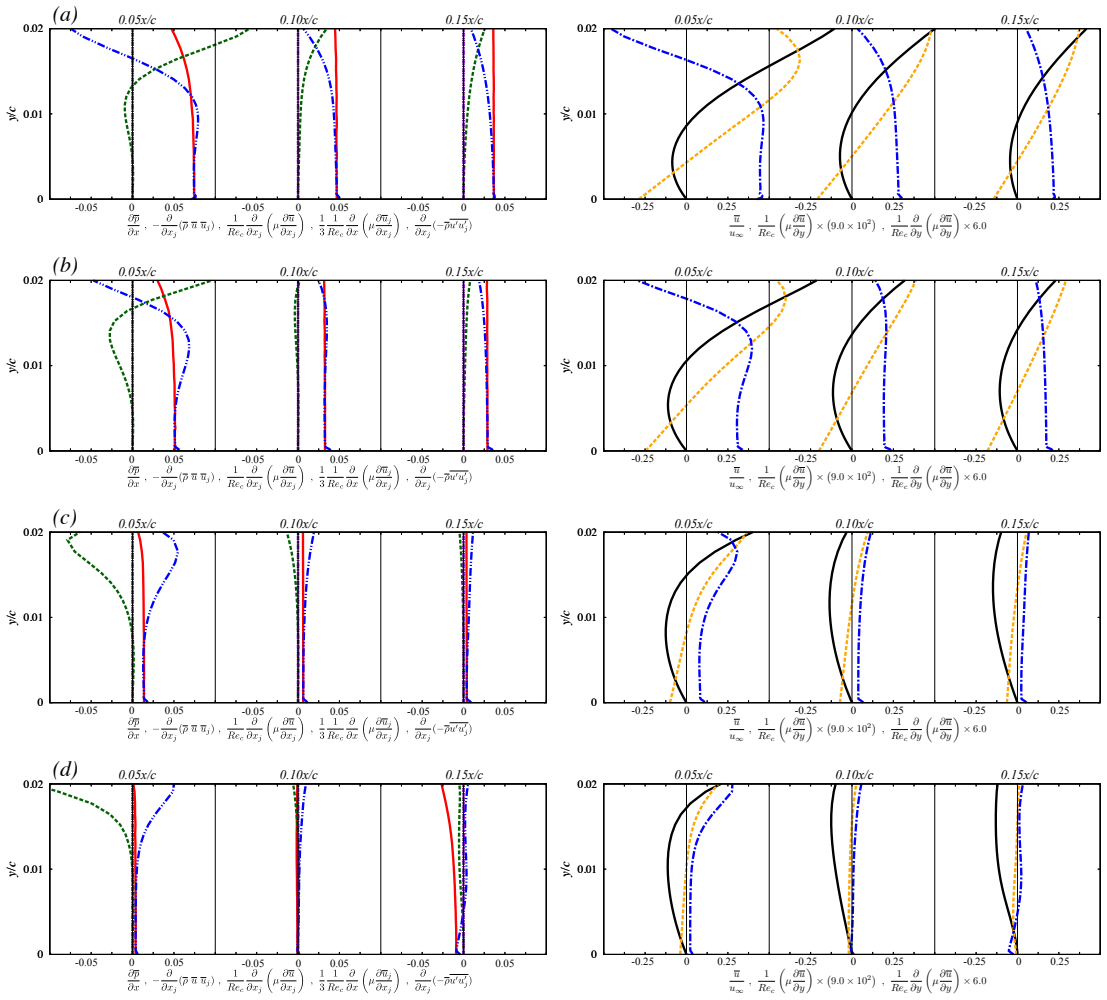

Figure 6. (Left) Momentum budgets in Eq. (2) in the wall-normal direction at several positions within the steady LSB region; Pressure gradient (red), convective (green), first viscous diffusion (blue), second viscous diffusion (black), and Reynolds stress (violet) terms. (Right) Time- and spanwise-averaged streamwise velocity (black), viscous stress (yellow), and viscous diffusion (blue) distribution at (a) $Re_c = 5.0 \times 10^3$, (b) $Re_c = 6.0 \times 10^3$, (c) $Re_c = 1.1 \times 10^4$, and (d) $Re_c = 2.0 \times 10^4$

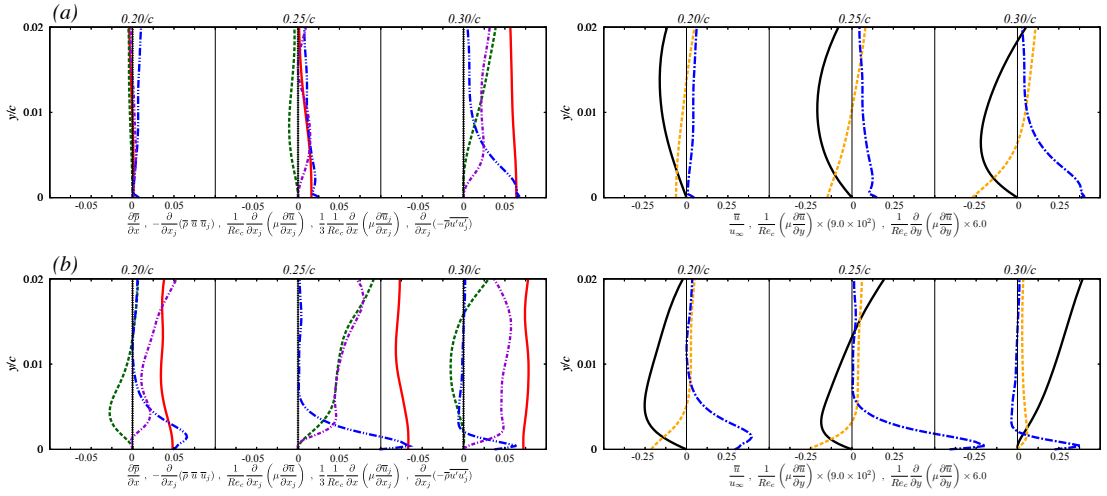

Figure 7. (Left) Momentum budgets in Eq. (2) in the wall-normal direction at several positions within the fluctuating LSB region; Pressure gradient (red), convective (green), first viscous diffusion (blue), second viscous diffusion (black), and Reynolds stress (violet) terms. (Right) Time- and spanwise-averaged streamwise velocity (black), viscous stress (yellow), and viscous diffusion (blue) distribution at (a) $Re_c = 1.1 \times 10^4$ and (b) $Re_c = 2.0 \times 10^4$